frontiers in Materials

ORIGINAL RESEARCH
published: 05 January 2022
doi: 10.3389/fmats.2021.790753

# Differently Charged P (VDF-TrFE) Membranes Influence Osteogenesis Through Differential Immunomodulatory Function of Macrophages

*Peijun Zhu[1†], Chunhua Lai[1†], Mingwei Cheng[1], Yiheng He[1], Yan Xu[1], Jiahao Chen[1], Zhengnan Zhou[2]*, Ping Li[1]* and Shulan Xu[1]**

[1]Center of Oral Implantology, Stomatological Hospital, Southern Medical University, Guangzhou, China, [2]School of Material Science and Engineering and National Engineering Research Center for Tissue Restoration and Reconstruction, South China University of Technology, Guangzhou, China

OPEN ACCESS

**Edited by:**
Vladimir Shvartsman,
University of Duisburg-Essen,
Germany

**Reviewed by:**
Wen Shi,
University of Nebraska Medical Center, United States
Lingqing Dong,
Zhejiang University, China

***Correspondence:**
Zhengnan Zhou
zn0810411329@scut.edu.cn
Ping Li
ping_li_88@smu.edu.cn
Shulan Xu
xushulan_672588@smu.edu.cn

[†]These authors have contributed equally to this work

**Specialty section:**
This article was submitted to Biomaterials, a section of the journal Frontiers in Materials

**Received:** 07 October 2021
**Accepted:** 14 December 2021
**Published:** 05 January 2022

**Citation:**
Zhu P, Lai C, Cheng M, He Y, Xu Y, Chen J, Zhou Z, Li P and Xu S (2022) Differently Charged P (VDF-TrFE) Membranes Influence Osteogenesis Through Differential Immunomodulatory Function of Macrophages. Front. Mater. 8:790753. doi: 10.3389/fmats.2021.790753

A biomaterial-mediated immune response is a critical factor to determine the cell fate as well as the tissue-regenerative outcome. Although piezoelectric-membranes have attracted considerable interest in the field of guided bone regeneration thanks to their biomimetic electroactivity, the influence of their different surface-charge polarities on the immune-osteogenic microenvironment remains obscure. The present study aimed at investigating the interaction between piezoelectric poly (vinylidene fluoridetrifluoroethylene) [P (VDF-TrFE)] membranes with different surface polarities (negative or positive) and macrophage response, as well as their subsequent influence on osteogenesis from an immunomodulating perspective. Specifically, the morphology, wettability, crystal phase, piezoelectric performance, and surface potential of the synthetic P (VDF-TrFE) samples were systematically characterized. In addition, RAW 264.7 macrophages were seeded onto differently charged P (VDF-TrFE) surfaces, and the culture supernatants were used to supplement cultures of rat bone marrow mesenchymal stem cells (rBMSCs) on the corresponding P (VDF-TrFE) surfaces. Our results revealed that oppositely charged surfaces had different abilities in modulating the macrophage-immune-osteogenic microenvironment. Negatively charged P (VDF-TrFE), characterized by the highest macrophage elongation effect, induced a switch in the phenotype of macrophages from M0 (inactivated) to M2 (anti-inflammatory), thus promoting the osteogenic differentiation of rBMSCs by releasing anti-inflammatory cytokine IL-10. Interestingly, positively charged P (VDF-TrFE) possessed pro-inflammatory properties to induce an M1 (pro-inflammatory) macrophage-dominated reaction, without compromising the subsequent osteogenesis as expected. In conclusion, these findings highlighted the distinct modulatory effect of piezoelectric-P (VDF-TrFE) membranes on the macrophage phenotype, inflammatory reaction, and consequent immune-osteogenic microenvironment depending on their surface-charge polarity. This study provides significant insight into the design of effective immunoregulatory materials for the guided bone regeneration application.

**Keywords: piezoelectric material, immunoregulation, guided bone regeneration, surface charge, macrophage, bone marrow mesenchymal stem cells**

## 1 INTRODUCTION

Guided bone regeneration (GBR) is recognized as a minimally invasive bone augmentation technique for the reconstruction of maxillofacial bone defects, involving a combined application of bone graft with a barrier membrane (Omar et al., 2019). The GBR barrier membrane not only maintains the space stability of the graft fillings but also prevents bone-healing areas from gingival-fibrous tissue invasion, thereby promoting new bone regeneration (Sasaki et al., 2021). To date, bioinert GBR barrier membranes have been used in clinical applications, including the alveolar bone defects secondary to periodontitis, tumor, and maxillofacial trauma (Omar et al., 2019; Balbinot et al., 2021). However, considering the biological mechanisms of GBR treatment, the barrier membranes with potential osteoinductivity are required to further improve new bone formation and regeneration.

Endogenous electrical signals are characterized by the promotion of bone growth and reconstruction, but they are compromised when bone defects occur (Hassler et al., 1977; Isaacson and Bloebaum, 2010; Liu et al., 2017). It is well known that an external electrical stimulation can promote bone healing by restoring the electrical potential at the site of the bone defect (Fonseca et al., 2019; Rohde et al., 2019). Whereas, the clinical application of this approach is limited by its poor efficiency and inconvenience (Zhang et al., 2018). To overcome this shortcoming, the implantation of inherently charged biomaterials is a promising strategy for providing localized electrical stimulation to precisely modulate bone regeneration (Rajabi et al., 2015; Zhang et al., 2018). Piezoelectric materials are characterized by a unique polarization performance that can be switched by mechanical stimulation or an external electric field (Tandon et al., 2018; Khare et al., 2020). After electric polarization in a direct-current (DC) electric field, the generation of aligned dipoles creates polarized charges distributed on the surface of piezoelectric materials (Lee et al., 2015; Khare et al., 2020). The application of these piezoelectric polymers can be considered in bone regeneration thanks to their biomimetic electroactivity and proved the promotion of osteogenesis by mimicking the endogenous electrical microenvironment both *in vitro* and *in vivo* (Zhou et al., 2016; Gorodzha et al., 2017; Tang et al., 2017; Chudinova et al., 2019; Wang et al., 2020). In that, piezoelectric membranes have also been concerned in the research and development of GBR barrier membranes (Teixeira et al., 2011; Bai et al., 2019). Especially, the *in vivo* osteogenic effect of piezoelectric barium titanate/poly (vinylidene fluoridetrifluoroethylene) [BTO/P (VDF-TrFE)] membrane, superior to PTFE (Poly tetra fluoroethylene) barrier membrane commonly used, inspires the potential clinical application of piezoelectric membrane (Bai et al., 2019). Nonetheless, the influence of the surface charge polarity of the piezoelectric materials (negative or positive charges) on their osteogenic performance has been controversially discussed. Zhang *et al.* demonstrated that the negatively charged poly (vinylidene fluoridetrifluoroethylene) [P (VDF-TrFE)] membranes with excellent biocompatibility induce osteogenesis both *in vitro* and *in vivo* (Zhang et al., 2018). Conversely, some conflicting reports revealed that positively charged substrates with piezoelectricity exert the most significant osteogenic effect on either osteoblasts (Vanek et al., 2016) or mesenchymal stem cells (MSCs) (Liu et al., 2017).

In principle, the implantation of biomaterial inevitably triggers an immune response mediated by the innate immune cells. The extent of this response plays a crucial role in the initiation of bone regeneration (Seebach and Kubatzky, 2019; Sadowska and Ginebra, 2020). In that, macrophages are recognized as forerunners to discern and respond to foreign biomaterials (Miron and Bosshardt, 2016; Ogle et al., 2016). During the early stages after implantation of biomaterials, the macrophages migrate to the implant area and differentiate into the pro-inflammatory M1 phenotype (classical type), triggering the defensive inflammation by the release of pro-inflammatory molecules, such as interleukin (IL)-1, tumor necrosis factor (TNF)-α and inducible nitric oxide synthase (iNOS) (Wu et al., 2020). The phenotype plasticity allows macrophages to switch into different phenotypes in response to distinct material signals (Miron and Bosshardt, 2016; Xu et al., 2020). Subsequently, anti-inflammatory M2 macrophages (alternative type) participate in bone reconstruction by the production of anti-inflammatory molecules, including arginase-1 (Arg-1), IL-10, and IL-4 (Wei et al., 2018). Moreover, the prolongation of the M1 phenotype state causes the rejection of the biomaterial, thereby compromising bone regeneration (Amengual-Penafiel et al., 2019). Under favorable conditions, the conversion of macrophage into the M2 phenotype ends the pro-inflammatory state and induces a beneficial immunological memory, in turn inducing a favorable osteogenic environment to accelerate bone repairing (Brown et al., 2017; Wang X. et al., 2021). Based on the above considerations, the regulative effect of biomaterials on macrophage-mediated osteogenesis is an important criterion for evaluating their potential for bone-regenerative application (Neacsu et al., 2014; Jin et al., 2019; Zhang et al., 2019). To date, only a few studies reported the regulation effect of piezoelectric materials on the immune-osteogenic microenvironment. The M2 macrophages could be induced by an electrical environment built by charged P (VDF-TrFE) coatings (Wang Z. et al., 2021). Nevertheless, an inconsistent result showed that the surface charges of piezoelectric PVDF could cause a M1 macrophage-dominated response, thus promising in the field of tumor immunotherapy (Kong et al., 2021). Moreover, previous studies demonstrated that the cation (positive potential) triggers inflammation, whereas the anion (negative potential) ameliorates the inflammatory response (Brodbeck et al., 2002; Ding et al., 2020; Xie et al., 2020). Based on the controversy regarding the macrophage response to the charged piezoelectric material, our hypothesis was that the surface-charge polarity (negative or positive) of the piezoelectric material might be an essential factor in determining the inflammatory response by macrophages.

Herein, given the potency of piezoelectric membranes to be applied for GBR treatment, it is imperative to clarify whether their different-charge characteristic could differentially affect the

macrophage behavior and thus osteogenesis, aiming to promote the development of piezoelectric GBR membranes. In the present study, the P (VDF-TrFE) membrane was used as an experimental material thanks to its good piezoelectricity for generating stable surface charges and excellent biocompatibility suitable for medical application (Zhang et al., 2018; Wang Z. et al., 2021). Moreover, negatively (poled -), positively (poled +), and neutrally (nonpoled) charged P (VDF-TrFE) membranes were fabricated, and their regulative effect on phenotype and inflammation of RAW 264.7 macrophages were determined. To further understand the critical role of macrophage response in the osteogenic differentiation induced by differently charged P (VDF-TrFE), rat bone marrow mesenchymal stem cells (rBMSCs) were further characterized after establishing an immune-osteogenic microenvironment model consisting of P (VDF-TrFE)–macrophage–BMSC using indirect co-culture method.

# 2 MATERIALS AND METHODS

## 2.1 Fabrication and Characterization of P (VDF-TrFE) Membranes

For fabrication of P (VDF-TrFE) membrane, a total of 3 g powdered P (VDF-TrFE) polymer (Arkema, Paris, France) were added to 20 ml N, N-dimethylformamide (Aladdin Chem Co., Ltd., Shanghai, China) and stirred at 60°C until the powder was entirely dissolved. The P (VDF-TrFE) solution was dripped onto a sandblasted titanium substrate, then placed in a drying oven at 80°C to allow the evaporation of the solvent, and it subsequently underwent isothermal crystallization, as described in our previous study (Zhou et al., 2016). A DC electric field (6 kV/cm, 60 min, 120°C) was used for poling the P (VDF-TrFE) membranes.

Scanning electron microscopy (SEM; Gemini 300, Zeiss, Germany) was used to analyze the surface morphology of the P (VDF-TrFE) membranes. The wettability of differently charged materials was measured using a water contact angle test. X-ray diffraction (XRD, SmartLab, Rigaku, Japan) and Fourier-transform infrared spectroscopy (FTIR, IRAffinity-1s, Shimadzu, Japan) were used to determine the crystal phase composition of the material before ("nonpoled") and after ("poled –" and "poled +") the poling treatment. The piezoelectric coefficient ($d_{33}$) of the P (VDF-TrFE) membranes immersed in DMEM for 6 weeks was measured using a piezoelectric response instrument (YE2730A, Sinoceramics, China) to determine the stability of piezoelectricity and electroactivity. Kelvin probe force microscopy (KPFM) measurements were conducted using the KPFM mode in a scanning probe microscope (Multimode 8, Bruker, Germany) to measure the relative surface potential of the poled P (VDF-TrFE) membranes, using the characteristics of neutrally charged P (VDF-TrFE) membrane ("nonpoled") as a reference. According to the charge characteristics of the membranes, this experiment was divided into "poled –," "poled +," and "nonpoled" groups, the latter used as the control group.

## 2.2 Macrophage Response to Differently Charged P (VDF-TrFE) Membranes

### 2.2.1 Direct Contact Test

RAW 264.7 cells (ATCC number: TIB-71, American Type Culture Collection, USA) were cultured in DMEM/high glucose media (Thermo Fisher Scientific, USA), supplemented with 10% fetal bovine serum (FBS, ExCell Bio, Shanghai, China) and 1% penicillin/streptomycin (Thermo Fisher Scientific, USA). The cells were digested and passaged using 0.25% trypsin (Thermo Fisher Scientific, USA) after reaching 80% confluence. The "nonpoled," "poled –," and "poled +" P (VDF-TrFE) membranes were disinfected overnight in 75% ethanol at room temperature, then exposed to ultraviolet light for 1 h prior to tests. The RAW 264.7 cells were then seeded on the different P (VDF-TrFE) membranes at a cell density of $2 \times 10^4$ cells/cm$^2$. After 3 days of culture, the phenotype and inflammation response of the macrophage was determined.

### 2.2.2 Cell Viability

Lactate dehydrogenase (LDH) levels were determined using the LDH assay kit (Beyotime Biotechnology, Shanghai, China) to clarify whether the presence of surface charges compromises cell viability. The culture supernatants were collected, and the LDH release was measured according to the manufacturer's instructions.

### 2.2.3 Cell Adhesion and Morphology

The number of macrophages adhering to the P (VDF-TrFE) membranes was assessed after being fixed with 4% paraformaldehyde. The nuclei were stained with 4,6-diamidino-2-phenylindole dilactate (DAPI) solution (Invitrogen, USA), the cells were visualized using a fluorescence microscope (DM4000B, Leica, Germany) and quantified using ImageJ software. The morphology of macrophages on the P (VDF-TrFE) membrane was observed by fluorescence microscopy, and the images were acquired after staining with both DAPI and fluorescein isothiocyanate (FITC)-phalloidin solution (Invitrogen, USA). The morphology was characterized by ImageJ by the determination of the cell surface area (μm$^2$), cell perimeter (μm), Feret's diameter (μm) and cell diameter aspect ratio (maximum diameter/minimum diameter, $D_{max}/D_{min,}$ %), as previously reported (McWhorter et al., 2013; Cipriano et al., 2015; Fahlgren et al., 2015).

### 2.2.4 Macrophage Phenotype Analysis

The surface markers of M1 (CCR7) and M2 (CD206) macrophages were analyzed using flow cytometry. After the removal of the RAW 264.7 cells from the P (VDF-TrFE) membranes, they were rinsed with phosphate buffered saline (PBS) and resuspended in 100 μl PBS ($1 \times 10^6$ cells per analysis tube). The cells were incubated with PE-labeled CD206 antibody (Biolegend, USA) and APC-labeled CCR7 antibody (Biolegend, USA) and analyzed by flow cytometry (Cytoflex, Beckman, USA). The distribution of the positive markers was evaluated using Flow Jo software.

**TABLE 1** | Primer sequences of qRT-PCR.

| Genes | Forward primer sequences (5′-3′) | Reverse primer sequences (5′-3′) |
|---|---|---|
| Mouse-iNOS | GTTCTCAGCCCAACAATACAAGA | GTGGACGGGTCGATGTCAC |
| Mouse-TNF-α | CTGAACTTCGGGGTGATCGG | GGCTTGTCACTCGAATTTTGAGA |
| Mouse-Arg-1 | TTGGGTGGATGCTCACACTG | GTACACGATGTCTTTGGCAGA |
| Mouse-IL-10 | GCTCTTACTGACTGGCATGAG | CGCAGCTCTAGGAGCATGTG |
| Mouse-GAPDH | AGGTCGGTGTGAACGGATTTG | TGTAGACCATGTAGTTGAGGTCA |
| Rat-ALP | CCTAGACACAAGCACTCCCACTA | GTCAGTCAGGTTGTTCCGATTC |
| Rat-GAPDH | GGCAAGTTCAACGGCACAGT | GCCAGTAGACTCCACGACAT |

### 2.2.5 Pro-/anti-inflammatory Protein Expression and Cytokine Secretion

The expression of M1/M2 macrophage-related protein iNOS and Arg-1 was detected by western blot analysis. Briefly, the total protein was extracted from RAW 264.7 cells using lysis buffer mixed with a protease inhibitor, and the concentration was quantified. For each group ("nonpoled," "poled −," and "poled +" groups), a total of 20 μg protein was separated by 12% SDS-PAGE, and the bands were transferred to PVDF membranes. The membranes were blocked by 5% bovine serum albumin (BSA), subsequently incubated with the GAPDH (Boster, China), iNOS and Arg-1 primary antibodies (Proteintech, China) overnight at 4°C, and then with the appropriate secondary antibody (Boster, China) for 1 h at room temperature. The PVDF membranes were rinsed with tris-buffered saline/Tween, the protein bands were visualized using enhanced chemiluminescence, and the images were captured. The protein expression was determined from the grayscale values of the protein bands using ImageJ software. The secretion of the pro/anti-inflammatory cytokines TNF-α, IL-10 was measured using Enzyme-linked immunosorbent assay (ELISA) kits (Elabscience, China). After 3 days of incubation, the cells were rinsed and then cultured in a serum starvation media for 6 h. Next, the supernatants were extracted and centrifugated for 10 min at 1,000 rpm and 4°C, followed with the storage at −80°C before use. The concentration of the above cytokines in each group was measured according to the manufacturer's instructions. The optical density (OD) of each well was measured using a microplate reader (ELX808, Bio-Tek, USA) at a wavelength of 450 nm.

### 2.2.6 Pro-/anti-inflammatory Gene Expression

The mRNA expression of pro-inflammatory genes (iNOS and TNF-α) and the anti-inflammatory ones (Arg-1 and IL-10) was quantified by quantitative real-time polymerase chain reaction (qRT-PCR). Briefly, the total RNA from macrophages was extracted using the TRIzol reagent (Invitrogen, USA) and then quantified using a Nanodrop 2000 spectrophotometer (Thermo Fisher Scientific, USA). An amount of 1,000 ng total RNA was used to synthesize cDNA using a FastKing gDNA Dispelling RT SuperMix kit (Tiangen, China). Next, RT-PCR was performed using a FastKing One-Step RT-qPCR kit (SYBR Green, Tiangen, China) by a PCR instrument (CFX Connect, Bio-Rad, USA). The primers used are listed in **Table 1**.

## 2.3 Osteogenic Differentiation of rBMSCs on Different P (VDF-TrFE) Surfaces in Conditioned Media

### 2.3.1 Conditioned Media Preparation and rBMSC Culture

We further investigated whether the macrophage response, mediated by differently charged P (VDF-TrFE) membranes, may influence the osteogenic differentiation of rBMSCs cultured on charged P (VDF-TrFE) membranes. As shown in **Figure 1**, the macrophage supernatants were collected as described above (the Materials and Methods 2.2.5) and were diluted one-fold with a fresh complete DMEM/F12 containing an osteogenic induction medium (Cyagen Biosciences, Guangzhou, China), thus constituting the conditioned media (CM) for each group, followed by the storage at −80°C before use. The rBMSCs (Cyagen Biosciences, Guangzhou, China) were seeded on P (VDF-TrFE) membranes at a density of $2 \times 10^4$ cells/cm$^2$, then cultured in DMEM/F12 media supplemented with 10% FBS and 1% penicillin/streptomycin. After 24 h of culture, the complete culture media was replaced with CM. rBMSCs were located in two environments, one represented by the P (VDF-TrFE) surfaces, and the other by the corresponding macrophage-CM, divided into the "poled −/CM," "poled +/CM" and "nonpoled/CM" groups. The rBMSCs cultured on the corresponding P (VDF-TrFE) membrane without CM were used as a control, named for the "poled -," "poled +" and "nonpoled" groups.

### 2.3.2 Cell Morphology

The DAPI nuclear staining and cytoskeleton-phalloidin staining were performed as mentioned above (the Materials and Methods 2.2.3) to determine whether the CM from the macrophage culture influenced the cell spreading of rBMSCs on differently charged P (VDF-TrFE) membranes at 1 and 3 days of culture. The results were observed by fluorescence microscopy.

### 2.3.3 Alkaline Phosphatase Staining and Gene Analysis

To clarify whether the CM from macrophage-P (VDF-TrFE) culture modulates osteogenic differentiation, alkaline phosphatase (ALP) staining and gene expression analysis were performed after 7 days of culture, as reported before (Purohit et al., 2020). In short, the cells were rinsed three times in PBS, fixed with 4% paraformaldehyde for 10 min, then incubated in

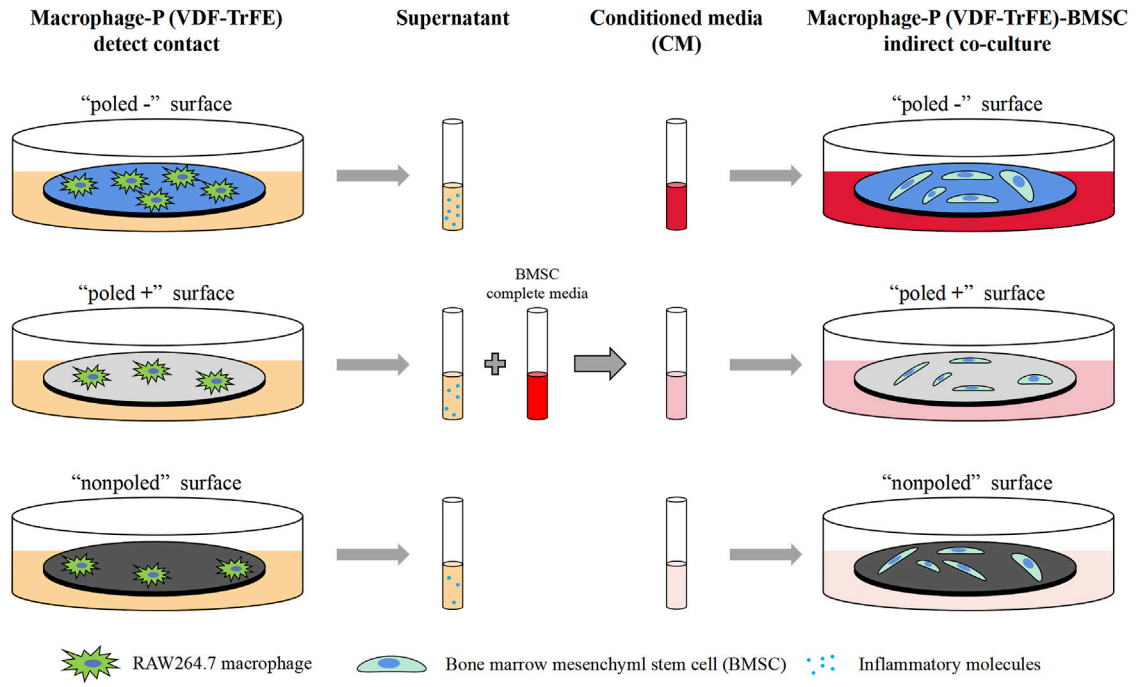


**FIGURE 1 |** Schematic illustration of the conditioned-media preparation. The supernatants were collected from macrophage-P (VDF-TrFE) culture and the conditioned media were further prepared to cultivate BMSCs.

ALP staining solution (Beyotime Biotechnology, Shanghai, China) at room temperature for 1 h. The gene expression was evaluated as described in paragraph 2.2.6 and the primers used are listed in **Table 1**.

### 2.3.4 Alizarin Red Staining

The culture of rBMSCs with or without CM was performed for 14 days. Then, the cells were washed in PBS, fixed, and the mineralized nodules produced by the rBMSCs were visualized by the incubation with 2% alizarin red solution (Cyagen Biosciences, China) at room temperature for 1 h. According to the manufacturer´s instructions, the mineralized nodules were quantified at 562 nm using a microplate reader.

## 2.4 Statistical Analysis

Statistical analysis was performed using SPSS 22.0 software (IBM Corporation, Chicago, USA). The results were expressed as mean and standard deviation. Where applicable, the Shapiro-Wilk test was performed to analyze the normal distributions of all experimental data sets. Statistical comparisons between two groups were calculated using a paired Student's t-test. Comparisons of three groups were performed using one-way analysis of variance (ANOVA) followed by post hoc Tukey's multiple comparison tests if normality tests passed. Non-parametric data sets were analyzed by the Kruskal-Wallis test followed by Bonferroni's multiple comparisons test. A $p$-value less than 0.05 was considered statistically significant.

# 3 RESULTS

## 3.1 P (VDF-TrFE) Membrane Characterization

The P (VDF-TrFE) membranes used in this study were approximately 50 μm in thickness. The P (VDF-TrFE) membranes were electrically poled, followed by the detection of the β-phase content and piezoelectric coefficient (d33) constant that are common parameters for characterizing the electroactivity of the piezoelectric materials to reflect whether the electrical poling successfully alters the direction of the electric dipoles (Bai et al., 2019; Khare et al., 2020). In addition, FTIR and XRD were used to determine the β-phase content of P (VDF-TrFE). After the poling treatment, both the "poled −" and "poled +" P (VDF-TrFE) displayed typical β-phase peaks (840 $cm^{-1}$, 1,400 $cm^{-1}$) in the FTIR mapping (**Figure 2A**). The XRD analysis (**Figure 2B**) revealed that the "poled -" and "poled +" P (VDF-TrFE) membranes had a more distinct peak at approximately 20° when compared to that of the nonpoled samples. This implies that the poled P (VDF-TrFE) had the high content of the β-phase, as previously reported (Zhang et al., 2018). The $d_{33}$ test results showed that the $d_{33}$ values increased from 0.4 pC/N to approximately 15 pC/N after the poling treatment. From the stability analysis of piezoelectric performance (**Figure 2C**), one-way ANOVA analysis demonstrated that the $d_{33}$ value of poled membrane did not change significantly with increased immersion time ($F(5, 12) = 2.987$, $p = 0.06$), stable at approximately 15 pC/N. The poled membranes possessed a macroscopic polarity, resulting

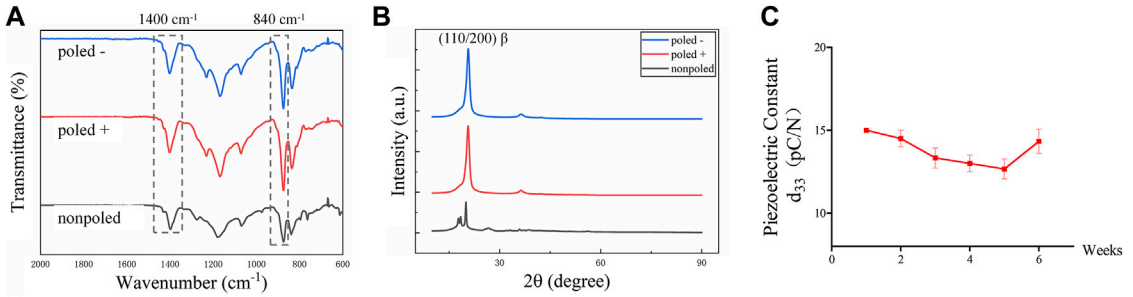


**FIGURE 2 |** Piezoelectric characterization of P (VDF-TrFE) membranes. **(A)** FTIR images and **(B)** XRD patterns for "poled –," "poled +" and "nonpoled" P (VDF-TrFE) samples, demonstrating the content of electroactive β-phase. **(C)** Piezoelectric coefficient (d33) of the poled P (VDF-TrFE) membranes immersed in DMEM for 6 weeks, indicating the stable electrical properties.

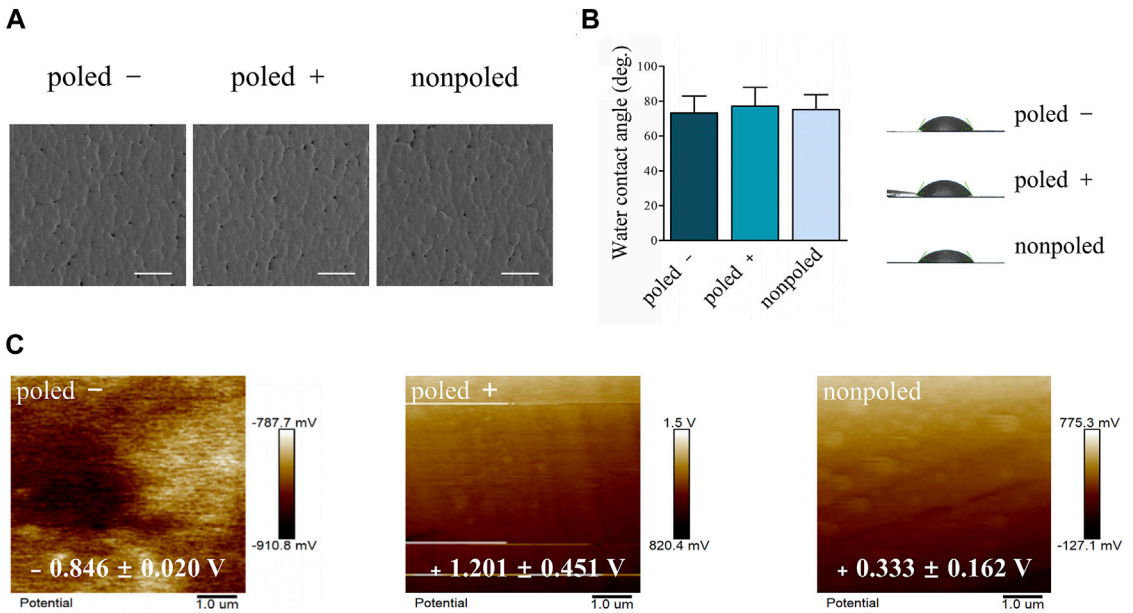


**FIGURE 3 |** Physical characterization of P (VDF-TrFE) membranes with different polarities. **(A)** Representative SEM micrographs at 500× magnification (scale bar: 50 μm). **(B)** Water contact angle analysis. **(C)** KPFM images displaying the relative surface potential distribution of the negatively, positively, and neutrally charged P (VDF-TrFE) membranes.

in a "poled –" face and a "poled +" face. The "poled -" and "poled +" faces were toward the negative and positive pole of the DC electric field and adsorbed the negative and positive polarized charges in terms of theory, respectively (Zhou et al., 2016; Khare et al., 2020; Dai et al., 2021).

The SEM images of the P (VDF-TrFE) membranes showed relatively smooth surfaces, indicating no apparent differences between "poled –," "poled +" and "nonpoled" surfaces (**Figure 3A**). Furthermore, statistical analysis by one-way ANOVA indicated no significant differences in water contact angles ($F(2, 6) = 0.040$, $p = 0.961$), with values of 73.20 ± 16.90°, 77.11 ± 18.66°, and 75.09 ± 14.83° for the "poled –," "poled +" and "nonpoled" surfaces, respectively (**Figure 3B**). The surface potential was further measured by KPFM to confirm the surface-charge polarities, as displayed in **Figure 3C**. The results revealed that the relative surface potential values of the "poled –," "poled +," and "nonpoled" were −0.846 ± 0.020 V, 1.20 ± 0.451 V, and 0.333 ± 0.162 V, respectively. The obtained negatively and positively charged P (VDF-TrFE) membranes were used as model materials for subsequent experiments, and the nonpoled membrane was used as the control group.

## 3.2 Macrophage Response to P (VDF-TrFE) Membrane *in vitro*

The ability of the differently charged P (VDF-TrFE) membranes to modulate the inflammatory behavior of macrophages was evaluated after 3 days of incubation. RAW 264.7 cells seeded on P (VDF-TrFE) membranes were used to determine cell adhesion, cell elongation, M1/M2 phenotype markers, the expression of the

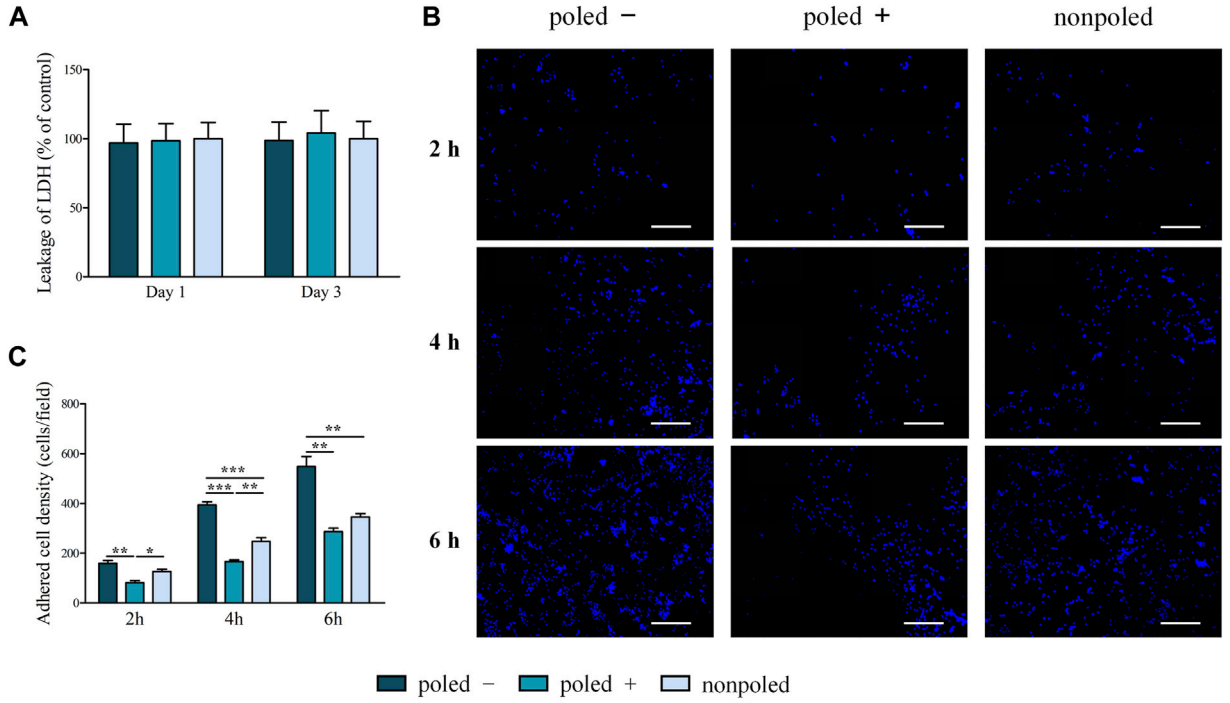


**FIGURE 4 |** Detection of cell adhesion and viability of macrophages cultured on P (VDF-TrFE) membranes. **(A)** Measurement of the LDH activity to evaluate the cell viability of the charged P (VDF-TrFE) membranes (neutrally charged surfaces as control). **(B)** Representative fluorescence images displaying the initial adhesion of macrophages on the P (VDF-TrFE) membranes after 2, 4, and 6 h of incubation (scale bar: 100 μm). **(C)** Quantification of adhesive cells. *$p < 0.05$; **$p < 0.01$; ***$p < 0.001$.

phenotype-related protein, the secretion of inflammatory cytokines, and the expression of inflammatory genes. Statistical analysis by one-way ANOVA showed no significant differences in LDH release among the different groups at 1 d ($F(2, 6) = 0.869$, $p = 0.466$) and 3 d ($F(2, 6) = 0.397$, $p = 0.689$) of culture (**Figure 4A**). Regarding the initial adhesion of macrophages as demonstrated by the fluorescence images and corresponding quantitative analysis, one-way ANOVA test exhibited significant differences in the macrophage adhesion induced by differently-charged surfaces at 2 h ($F(2, 6) = 16.778$, $p = 0.003$), 4 h ($F(2, 6) = 89.126$, $p < 0.0001$) and 6 h ($F(2, 6) = 27.810$, $p = 0.001$) of incubation. The pairwise comparisons showed a higher number of DAPI-positive cells were attached to the "poled −" surface when compared to those attached to the "poled +" ($p < 0.001$) or "nonpoled" ($p < 0.001$) surfaces after 4 h of incubation (**Figures 4B,C**).

Regarding cell-morphology images, RAW 264.7 cells cultured on the "poled −" surface possessed an elongated morphology, in comparison to the cells on the "poled +" and "nonpoled" surfaces showing a round shape with filopodia (**Figure 5A**). Generally, the cell elongation is characterized by the quantitative analysis of cell aspect ratio. The Kruskal-Wallis test showed a significant difference in cell aspect ratio among the different groups ($H(2) = 21.998$, $p = 0.00002$). Specifically, Bonferroni's multiple comparisons showed a significantly higher ratio in the "poled −" (3.01 ± 1.65%) group when compared to the "nonpoled" (1.33 ± 0.31%, $p < 0.001$) and "poled +" (1.93 ± 1.06%, $p < 0.05$) groups (**Figure 5B**). Meanwhile, the "poled −" and P (VDF-TrFE) resulted in increased cell area, perimeter and Feret's diameter (**Figures 5C–E**), indicated by the statistical result of Kruskal-Wallis test for cell perimeter ($H(2) = 30.931$, $p < 0.001$) and Feret's diameter ($H(2) = 32.250$, $p < 0.001$) and one-way ANOVA test for cell area ($F(2, 42) = 22.100$, $p < 0.001$).

Flow cytometry was used to confirm the dominant phenotype of macrophages, showing a significant difference in M1 ($F(2, 6) = 33.363$, $p = 0.001$) and M2 ($F(2, 6) = 9.689$, $p = 0.013$) macrophage phenotypes induced by the three surface types. According to Tukey's multiple comparisons, the "poled −" group exhibited the highest proportion of CD206-positive M2 macrophages (17.57 ± 5.41%) than the "poled +" (6.86 ± 4.37%, $p < 0.05$) and "nonpoled" (3.74 ± 0.71%, $p < 0.05$) groups. Furthermore, the proportion of CCR7-positive M1 macrophages significantly increased from 3.19 ± 4.70% in the "nonpoled" group to 26.47 ± 3.87% in the "poled +" group ($p < 0.01$) (**Figures 6A,B**). Moreover, the results of cytokines secretion measured by ELISA revealed that IL-10 secretion was shown to be significantly increased in RAW264.7 cells cultured on the "poled −" surface ($p < 0.01$), whereas the highest secretion of TNF-α was observed in the "poled +" group ($p < 0.01$) (**Figure 6C**).

Additionally, the inflammatory protein determined by western blot revealed that the expression of anti-inflammatory Arg-1 protein ($F(2, 6) = 9.134$, $p = 0.015$) and pro-inflammatory iNOS protein ($F(2, 6) = 8.722$, $p = 0.017$) was significantly different among the different groups. Subsequently, Tukey's multiple comparisons exhibited an increased expression level of Arg-1 in the "poled −" group compared with the "poled +" and "nonpoled" groups ($p < 0.05$). On the contrary, the stimulation of the "poled +" surface

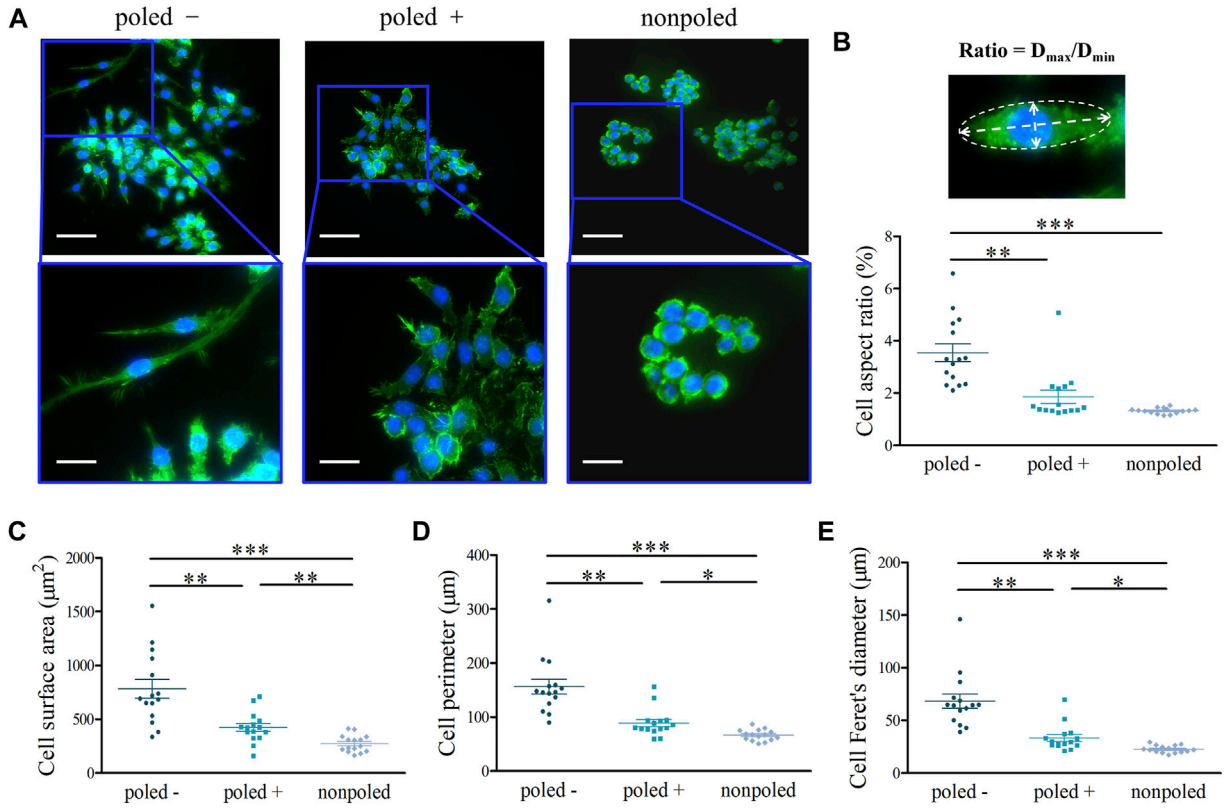


**FIGURE 5 |** Macrophage morphology and elongation. **(A)** Representative fluorescence images of the morphology of RAW 264.7 macrophages after the nucleus (blue) and cytoskeleton (green) staining (top scale bar: 50 μm, bottom scale bar: 25 μm). **(B)** Cell diameter aspect ratio ($D_{max}/D_{min}$) obtained by the cell morphology analysis, and the fluorescence images simply illustrating the cell-diameter measurement. Quantitative analysis of **(C)** cell surface area, **(D)** cell perimeter and **(E)** Feret's diameter. *$p < 0.05$; **$p < 0.01$; ***$p < 0.001$.

significantly increased iNOS protein expression ($p < 0.05$) (**Figures 6D,E**). Concerning the gene expression analysis, statistically significant differences of the gene expression of Arg-1 (H (2) = 17.623, $p = 0.0001$), IL-10 (H (2) = 17.464, $p = 0.00012$), iNOS (H (2) = 8.802, $p = 0.012$) and TNF-α (H (2) = 18.224, $p = 0.0001$) were confirmed by Kruskal-Wallis test. Post hoc pairwise comparisons showed a significantly higher Arg-1 and IL-10 expression in the RAW264.7 cells cultured on the "poled −" surface compared to the "poled +" ($p < 0.01$) and "nonploed" ($p < 0.001$) surfaces, whereas a significantly higher iNOS expression in the "poled +" surface compared to the "poled −" ($p < 0.05$) and "nonploed" ($p < 0.05$) surfaces. The expression of TNF-α was significantly increased upon the stimulation of the "poled +" surface when compared with the "poled -" surface ($p < 0.001$) (**Figure 6F**).

## 3.3 Association Between Macrophage Response and Osteogenic Differentiation of rBMSCs on P (VDF-TrFE) Membrane

The supernatants of the macrophage cultures on differently charged P (VDF-TrFE) membranes were used to prepare the CM to stimulate the rBMSCs cultured on the corresponding P (VDF-TrFE). From cell-fluorescence images, the rBMSCs were prone to attach on the P (VDF-TrFE) surfaces at 1 d of culture with the CM incubation, compared with the corresponding control groups (without the CM incubation). However, there was no distinct difference in the adhesive cells among the different groups at 3 d of culture, regardless of the CM stimulation. These indicated that the CM from macrophages cultured on the differently charged surfaces might be more conducive to the initial adhesion of rBMSCs on the corresponding surfaces. Additionally, the rBMSCs on the "poled −" and "poled−/CM" condition obviously spread better than those on the other four groups at 1 and 3 d of culture, with the most remarkable spreading shape in the "poled−/CM" group of 3 d (**Figure 7**).

ALP, as an early-essential indicator of BMSC differentiation to osteoblast (Wang et al., 2017), was stained in this work to investigate the osteogenic ability of macrophage-CM and charged P (VDF-TrFE) membranes. Both the macroscopic and microscopic images showed that ALP staining was increased in the "poled −" and "poled −/CM" groups, and the most distinct effect was observed in the rBMSCs cultured on the "poled −" surface upon CM stimulation. Otherwise, the CM from "poled +" surface-macrophage culture slightly increased ALP staining of rBMSCs on the "poled +" surface (**Figure 8A**). Regarding the ALP gene expression, it demonstrated no significant differences in ALP expression among the three groups without CM stimulation

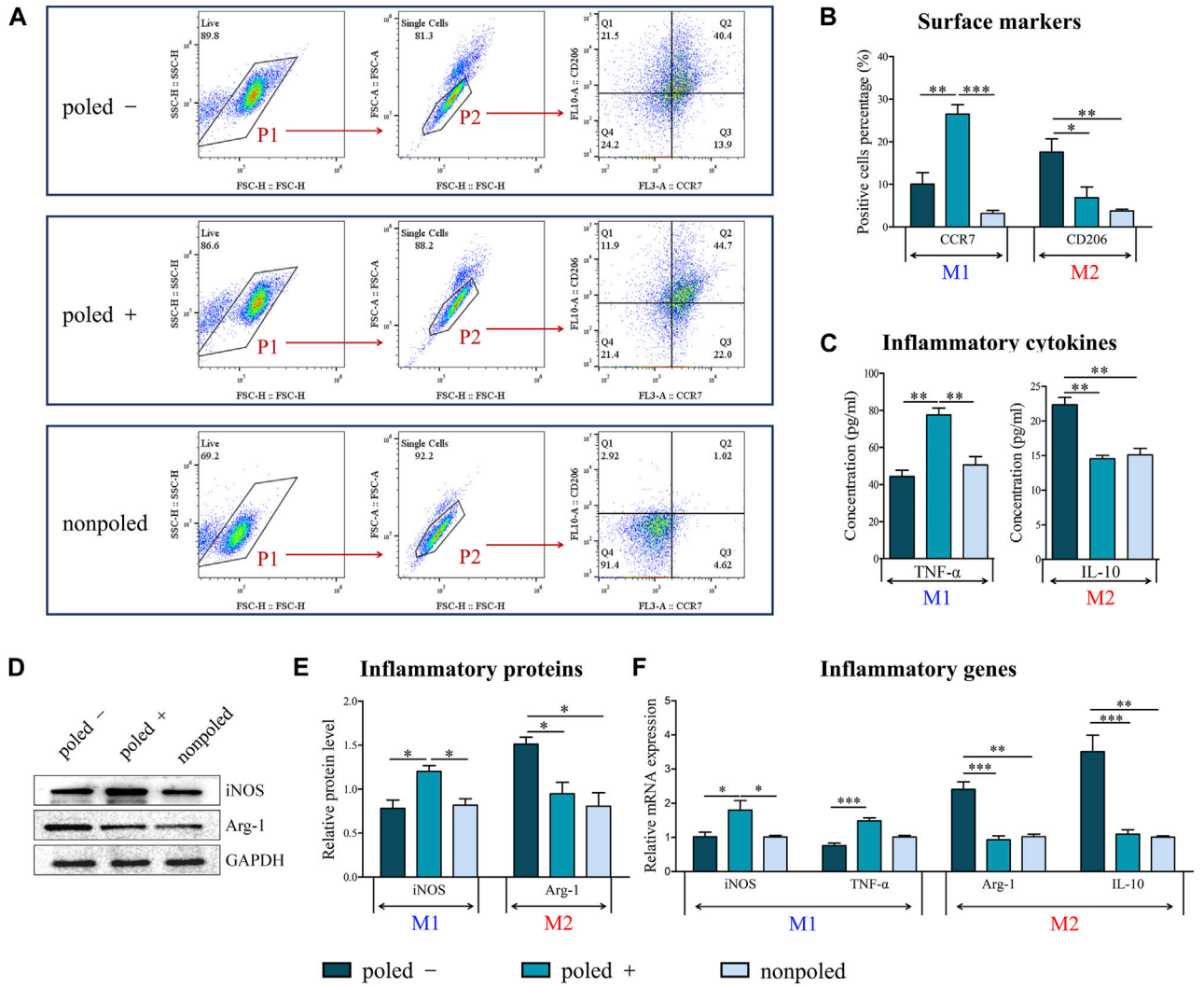


**FIGURE 6 |** Phenotype analysis of RAW 264.7 macrophages. **(A)** Flow cytometric analysis of the M1 macrophage marker CCR7 and the M2 macrophage marker CD206. **(B)** Quantitative analysis of CD206 and CCR7-positive cells by flow cytometry analysis. **(C)** Secretion of inflammatory cytokines as measured by ELISA. **(D)** Western bolt analysis of the inflammatory proteins iNOS and Arg-1. **(E)** Quantification of proteins by western blot analysis (GAPDH served as the internal control). **(F)** The expression of inflammatory genes as measured by qRT-PCR ("nonpoled" group as control). $^{*}p < 0.05$; $^{**}p < 0.01$; $^{***}p < 0.001$.

(H (2) = 3.227, $p = 0.199$), as well as the highest ALP expression in the "poled −/CM" group compared to the "poled +/CM" and "nonpoled/CM" groups (F (2, 6) = 16.632, $p = 0.004$). ALP gene expression of rBMSCs on the "poled −" surface was significantly enhanced by the addition of the corresponding CM ($p < 0.05$) (**Figure 8C**). The alizarin red-staining images showed that the rBMSCs on the "poled -" surface generated a greater number of mineralized nodules than that on the "poled +" and "nonpoled" surfaces after 14 days of culture, regardless of CM stimulation. Interestingly, the staining was slightly enhanced in the "poled +/CM" group compared with the "poled +" group (**Figure 8B**). The quantitative analysis by ANOVA confirmed the higher mineralized nodule-generative ability of rBMSCs on the "poled -" surface when compared with the other two surfaces without CM stimulation (F (2, 6) = 18.759, $p = 0.003$), as well as the most generated mineralized nodules in the "poled −/CM" group when compared with the "poled +/CM" and "nonpoled/CM" groups (F (2, 6) = 53.630, $p = 0.0001$). The CM from the "poled −" surface-macrophages culture further increased the generation of mineralized nodules of rBMSCs on the "poled −" surface ($p < 0.05$) (**Figure 8D**).

## 4 DISCUSSION

In the field of biomaterial medicine, numerous previous studies demonstrated that macrophages, as the primary innate immune cell type, play a pivotal role in the material-mediated immune response, thus determining the outcome of tissue regeneration (Miron and Bosshardt, 2016; Sadowska and Ginebra, 2020) and

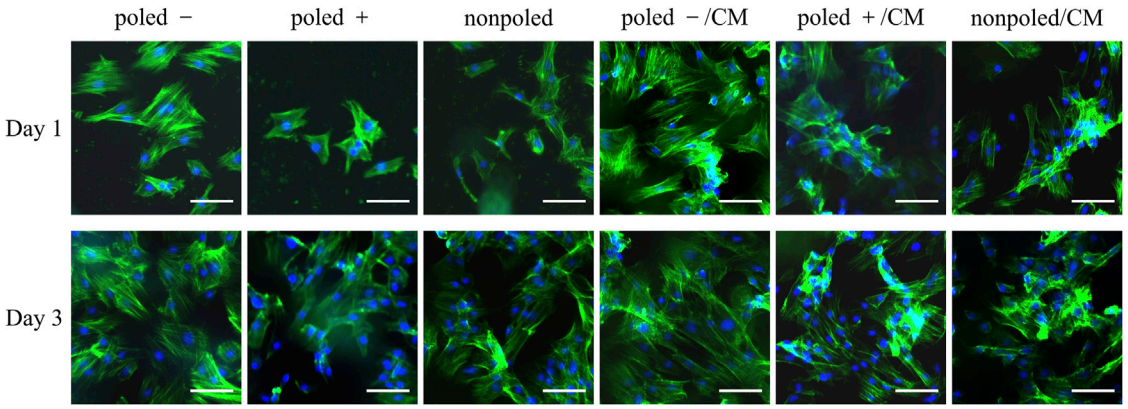


**FIGURE 7 |** Representative fluorescence microscopy images of rBMSCs cultured in normal media or conditioned media for 1 and 3 days. Blue fluorescence represents the nucleus stained with DAPI, and the green fluorescence indicates the cytoskeleton, stained with phalloidin (scare bars: 50 μm).

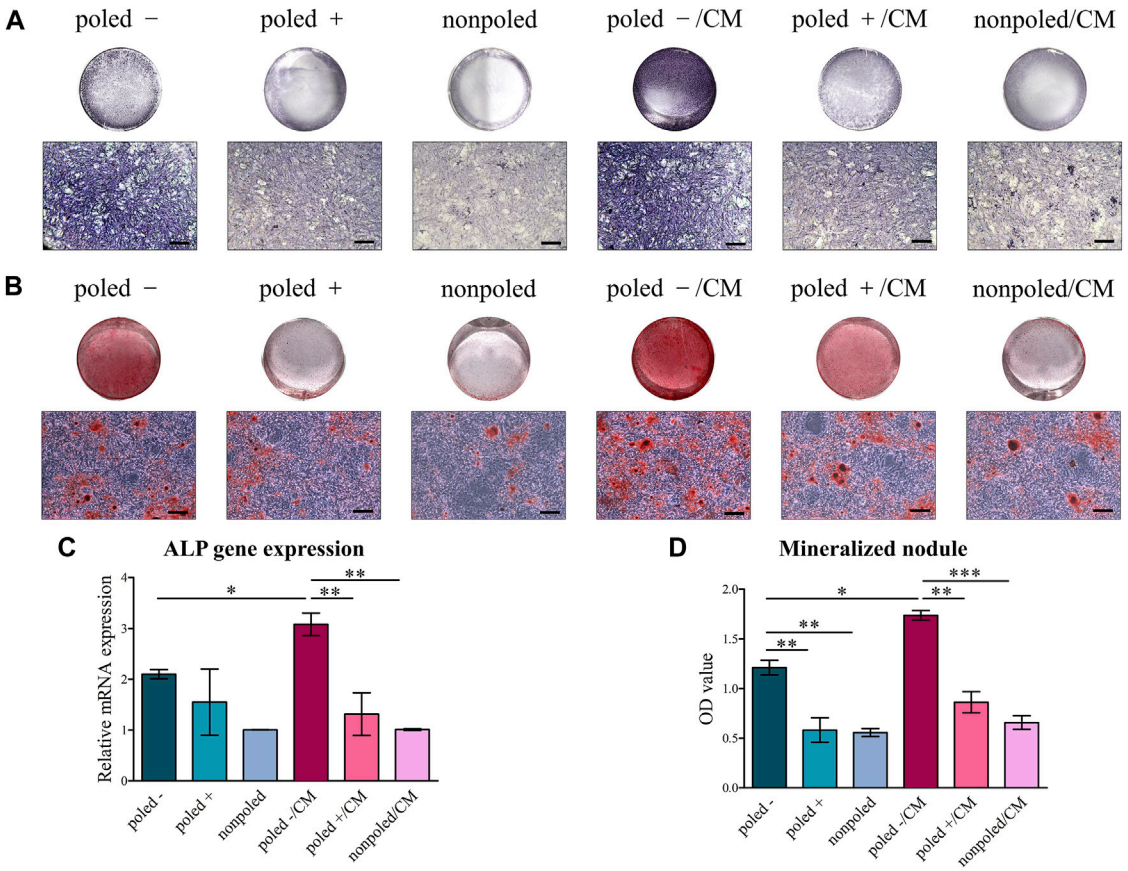


**FIGURE 8 |** Osteogenic differentiation of rBMSCs cultured on P (VDF-TrFE) membranes with/without CM. **(A)** Alkaline phosphatase staining of rBMSCs after 7 days of induction (top: macroscopic images, bottom: microscopic images, scare bar: 100 μm). **(B)** Alizarin red staining of rBMSCs after 14 of induction (top: macroscopic images, bottom: microscopic images, scale bar: 100 μm). **(C)** Expression of the osteogenic gene ALP ("nonpoled" group as control). **(D)** Quantitative analysis of the mineralized nodules by alizarin red staining. $^{*}p < 0.05$; $^{**}p < 0.01$; $^{***}p < 0.001$.

tumor immunotherapy (Zhang et al., 2020; Kong et al., 2021). Macrophages are characterized by remarkable plasticity, exhibiting different phenotypes with distinct functions under varying material stimulation. The M1 pro-inflammatory macrophages activate the inflammatory response and inhibit bone healing, whereas the M2 anti-inflammatory macrophages suppress the inflammation

induced by foreign materials, providing a favorable osteogenic environment (Ogle et al., 2016; Brown et al., 2017). Additionally, an electrical signal can mimic the endogenous electrical microenvironment, promoting wound healing, bone reconstruction (Rohde et al., 2019; Khare et al., 2020), and nerve regeneration (Cangellaris and Gillette, 2018; Fonseca et al., 2019). Hence, inherent electroactive biomaterials, especially piezoelectric materials, received wider attention in search of an appropriate electrostimulation therapy (Rajabi et al., 2015; Zhang et al., 2018; Toledano-Osorio et al., 2021). Previous numerous studies demonstrated the osteoinductivity of piezoelectric materials through a direct-contact testing, in which the surface properties directly affect the bone-related cells (Marchesano et al., 2015; Zhang et al., 2018). Nonetheless, to the best of our knowledge, only a few studies focused on the effect of charged-piezoelectric materials on the immune-osteogenic microenvironment. To date, it remains obscure how the piezoelectric membranes with different surface polarities affect the immune-osteogenic microenvironment. Based on the consideration above, representative piezoelectric P (VDF-TrFE) membranes for the GBR application were used as a model material. In addition, the macrophage response to the differently-physical charge of piezoelectric P (VDF-TrFE) membranes was determined. Furthermore, the potential osteoinduction and osteoimmunology properties were further demonstrated through the establishment of the material-macrophage-BMSC microenvironment.

## 4.1 Macrophage Adhesion and Morphology Affected by the Surface-Charge Polarity of P (VDF-TrFE) Membranes

In the present study, the electrical dipoles of piezoelectric P (VDF-TrFE) were generated by electrical poling treatment, thus creating net surface charges on the surfaces. The results were indirectly reflected by the increased β-phase contents and $d_{33}$ values, in line with previous studies (Zhang et al., 2018; Khare et al., 2020; Dai et al., 2021). Moreover, the wettability is a critical factor in determining cell behavior, which can be influenced by the surface topography and roughness (Kim et al., 2016; Kumar and Hiremath, 2019). Based on our results of surface topography and surface roughness measured by previous studies (Zhang et al., 2018; Bai et al., 2019), there were no significant differences in surface roughness and topography of P (VDF-TrFE) membranes before and after poling treatment. No alternations in surface roughness and topography may lead to the effect that no significant differences in water contact angle of differently charged P (VDF-TrFE) surfaces. Therefore, the interference of the topography and wettability of biomaterials with the behavior of macrophages reported in numerous studies (Hotchkiss et al., 2016; Hamlet et al., 2019) were excluded in this work. Combining surface-potential results to analyze, the three P (VDF-TrFE) membranes with similar surface topography and wettability but different surface charge polarity, such as negatively (poled -), positively (poled +) and neutrally (nonpoled) charged P (VDF-TrFE) membranes, were fabricated in this study. Herein, macrophage function is mainly determined by the surface-charge polarity of P (VDF-TrFE) membranes.

After demonstrating no cytotoxicity due to the surface charges, a direct contact test (*i.e.,* seeding cells directly onto the material's surface) was applied to observe the adhesion and morphology of macrophages on the P (VDF-TrFE) surface. Notably, RAW 264.7 macrophages were more prone to adhere on the negatively charged surface, in accord with previous study demonstrating that the stronger cell adhesion with larger focal adhesions (FAs) was found on the negatively charged surface of piezoelectric Lithium Niobate, compared with the positively charged surface (Marchesano et al., 2015). These results might be explained by the ion attraction in the electric double layer (Marchesano et al., 2015; Chen et al., 2017; Chakraborty et al., 2020). In other words, when the negatively charged surface was in direct contact with macrophages in the ion-containing media, cations ($Ca^{2+}$, $Mg^{2+}$) were predominantly adsorbed on the surface, thereby attracting electronegative cell adhesion proteins that were distributed on the cell membrane and exhibited divalent cation-dependent ligand binding (Hynes, 1987; Marchesano et al., 2015). However, the absence of divalent cation adsorption on the positively and neutrally charged surfaces caused a weaker bond with macrophages. The association between cell adhesion and cell shape has been reported, suggesting that the cell shape is stretched under strong adhesive forces and spherical under poor adhesive forces (Ribeiro et al., 2020). Additionally, a report showed that charged PVDF polymer could promote cell elongation (Ribeiro et al., 2020), and our findings are in accordance with these results. The results obtained by cell surface area, perimeter, Feret's diameter and aspect ratio showed that RAW 264.7 macrophages seeded on the negative surface possessed more elongated morphologies when compared to the round-shaped macrophages with filopodia on the positive and nonpoled surfaces. Unlike other cells, the distinct morphology of macrophages symbolizes and even influences their biological behaviors and functional state (Kang et al., 2017; Yang et al., 2021b). Indeed, the elongation of macrophages triggers the M2 phenotypic state and induces the secretion of anti-inflammatory molecules (McWhorter et al., 2013). These findings mentioned above indicate that the adhesive property of macrophages depend not only on the presence of the surface charges of the piezoelectric P (VDF-TrFE), but also on their surface charge polarity, with the highest cell adhesion and cell elongation effect of the negative surface.

## 4.2 Differently Charged P (VDF-TrFE) Membranes Characterized by Discrepant Preferences in Regulating the Macrophage-Immune Response

Undoubtedly, an appropriate macrophage phenotype induced by biomaterials is a prerequisite for immunotherapeutic materials in specific biomedical applications. The *in vitro* influence of differently charged P (VDF-TrFE) on the macrophage phenotype and functional secretion must therefore be determined. The RAW 264.7 cells on the negatively charged surface exhibited a predominant proportion of $CD206^+$ M2 macrophages, indicating that M2 macrophage-dominated reaction was induced, in contrast to the M1 macrophage-

mediated inflammation induced by the positively charged surface up-regulating the proportion of $CCR7^+$ M1 macrophages. Correspondingly, macrophages with different phenotypes secret diverse functional molecules to modulate subsequent tissue repairing processes (Ogle et al., 2016; Chen et al., 2020). Among these inflammatory molecules, TNF-α and iNOS with pro-inflammatory effects compromise bone healing, whereas Arg-1 and IL-10 with anti-inflammatory effects increase the reaction against foreign bodies and induce osteogenesis (Ogle et al., 2016; Ding et al., 2020). Both pro-inflammatory iNOS and TNF-α expression were the highest on the positive surface. Nevertheless, RAW 264.7 cells on the negative surface significantly possessed the highest Arg-1 expression and IL-10 secretion as well as the lowest iNOS expression, consistent with the phenotype analysis mentioned above. In addition, the qRT-PCR analysis further confirmed that the negatively and positively charged P (VDF-TrFE) induced the anti-inflammatory and pro-inflammatory response of macrophages, respectively.

Based on our results, negatively charged membranes induced macrophage phenotype from M0 to M2, probably contribute to the following factors. The negatively charged surface adsorbing divalent cations created a double electric layer (Marchesano et al., 2015), thereby promoting cell adhesion and elongation (Ribeiro et al., 2020), which ultimately determine the macrophage phenotype and functional secretion (McWhorter et al., 2013). Thangam *et al.* manipulated the adhesive protein of macrophages to reveal that the enhanced cell adhesion and elongation of macrophages can induce an M2 macrophage-dominated reaction (Thangam et al., 2021). Cell elongation without exogenous interference leads to the prominent M2 phenotype environment and anti-inflammatory molecules secretion by activating the rho-associated protein kinase (ROCK) signaling pathway (McWhorter et al., 2013; Yang et al., 2021c; Thangam et al., 2021). The immunoregulatory properties of the negatively charged P (VDF-TrFE) were in agreement with previous studies suggesting that synthetic polymer particles with negative charges reduce the immune response of macrophage and inhibit the inflammatory secretion by down-regulating the Toll-like receptor (TLR)-4 signaling pathway (Casey et al., 2019). In addition, the positively charged P (VDF-TrFE) exhibited positive surface potential that restricted the adhesion of proteins as well as cells (Dubey and Basu, 2014; Khare et al., 2020), activated the inflammatory response of macrophages (Brodbeck et al., 2002), and stimulated the pro-inflammatory TNF-α secretion (Liu et al., 2014). However, the exact mechanism still remains to be studied in depth.

## 4.3 The *In Vitro* Osteogenesis Mediated by Macrophage-Surface Charge Interaction on P (VDF-TrFE) Membranes

It is well-known that MSCs are sensitive to the charges of piezoelectric P (VDF-TrFE) polymers, which have been considered as potential promising bone regenerative materials (Zhang et al., 2018; Khare et al., 2020). Nevertheless, the *in vivo* and *in vitro* osteogenic effect of biomaterials are often inconsistent due to the discrepancies between *in vitro* cell culture conditions and *in vivo* complex physiological environments involving the host immune response to "foreign" biomaterials and its subsequent interaction with the skeletal system (Seebach and Kubatzky, 2019; Ding et al., 2020). Therefore, the *in vitro* studies of P (VDF-TrFE) polymers must focus on the type of immune response they cause and whether this response affects the subsequent osteogenesis.

In this study, after the preparation of the CM with the supernatants from macrophages cultured on different P (VDF-TrFE) surfaces, the ability of CM on affecting the interaction between the charged P (VDF-TrFE) and the rBMSCs was further investigated. The results demonstrated that the negatively charged P (VDF-TrFE) accelerated cell adhesion and cell spreading without CM incubation, which was consistent with a previous report indicating that MSCs can favor the adhesion and the spreading morphology on negatively P (VDF-TrFE) (Zhang et al., 2018). The CM from macrophage-negatively P (VDF-TrFE) is characterized by M2-anti-inflammatory properties as mentioned above, thus synergistically enhancing the effect of the negatively P (VDF-TrFE) on rBMSC spreading. The CM from M2 macrophages has been reported to enhance the secretion of extracellular matrix (ECM) components, especially COL-1 and integrin β1 proteins, thereby promoting rBMSC attachment and differentiation reflected by cell spreading (He et al., 2018; Peng et al., 2020; Tang et al., 2021). Moreover, the osteogenic differentiation induced by differently charged surfaces-macrophage CM was further confirmed by the mineralized nodule, ALP staining and ALP gene expression (Salamanca et al., 2021). Simply considering the direct effect of differently charged P (VDF-TrFE) on osteogenic differentiation of rBMSCs, the rBMSCs induced by the negatively P (VDF-TrFE) surface exhibited the most production of mineralized nodules and ALP protein, in accordance with the previous study suggesting a favorable osteogenic property of the negatively charged P (VDF-TrFE) (Zhang et al., 2018). After taking the macrophage-CM into consideration, a remarkably enhanced generation of ALP protein and mineralized nodules was observed, as well as ALP gene expression in the negative P (VDF-TrFE)-CM-BMSC co-culture compared with the negative P (VDF-TrFE)-BMSC mono-culture, indicating that the macrophage response was essential for the negatively charged P (VDF-TrFE) to exert a pro-osteogenic effect. These phenomena might be explained by a considerable level of IL-10 secretion induced by the negative P (VDF-TrFE), promoting the osteogenic differentiation of rBMSCs through the supernatant stimulating method. IL-10 secretion is a confirmed molecular mechanism used by M2 macrophage-CM to promote the osteogenic differentiation of MSC, and the inhibition of IL-10 compromises the osteogenic effect of M2 macrophage-CM (Valles et al., 2020).

Interestingly, although M1 macrophage-CM damaging osteogenesis has been widely reported (He et al., 2018; Biguetti et al., 2021), some recent reports showed that the low inflammatory M1 macrophage state (Yang L. et al., 2021) and low concentration of TNF-α (Valles et al., 2020) play a vital role in the osteogenic differentiation of MSC. Herein, the M1 macrophage-dominated response mediated by the positive

P (VDF-TrFE) did not compromise the osteogenic differentiation of rBMSCs and even slightly enhanced mineralized nodule generation. In summary, the surface-charge polarity (negative or positive) of piezoelectric P (VDF-TrFE) resulted as an important parameter to determine the immune-osteogenic environment as it affected macrophage-inflammatory behaviors, which in turn influenced rBMSC osteogenic activity. These findings illustrate an indispensable role of the macrophage response to electroactive P (VDF-TrFE) in regulating osteogenesis and thus emphasize the critical role of the immune-osteogenic environment and the need of multicellular co-culture (direct or indirect) with biomaterials whose *in vivo* fate was determined jointly by a multi-system and multi-cell (Chen et al., 2019; Sadowska and Ginebra, 2020). Therefore, although the disparate immunoregulatory preferences of differently charged P (VDF-TrFE) membranes have been observed, the mechanisms by which piezoelectric-charged material interacted with macrophage and modulated immune-osteogenic microenvironment are still not fully understood and should be further investigated.

## 5 CONCLUSION

In this study, three types of charged P (VDF-TrFE) surfaces (negative or positive, and neutral as control) were fabricated and characterized, highlighting how the charge polarities of the piezoelectric P (VDF-TrFE) induced the switching in macrophage phenotype and immune-osteogenic microenvironment. Discrepant preferences of differently charged P (VDF-TrFE) in modulating the macrophage-inflammatory response were elucidated, indicating that the negatively and positively charged P (VDF-TrFE) drove macrophages towards the M1 pro-inflammatory and M2 anti-inflammatory states, respectively. Furthermore, an immune-osteogenic microenvironment model consisting of P (VDF-TrFE)–macrophage–BMSC was established using indirect co-culture with macrophage CM. The results showed that the negatively charged P (VDF-TrFE) with direct pro-osteogenic effect also elicited the release of M2-anti-inflammatory cytokines by macrophages to act on rBMSCs, thereby synergistically inducing the osteogenic differentiation. The positively charged P (VDF-TrFE)-mediated M1 pro-inflammatory condition did not damage the rBMSC osteogenesis on the corresponding surface as expected. To sum up, the differently charged piezoelectric materials had discrepant preferences in regulating the inflammatory phenotype switching and functional secretion of macrophages, thereby impacting osteogenesis in a different way. The negatively charged-P (VDF-TrFE) membrane has a superior regulation effect on the immune-osteogenic microenvironment. These findings have significant implications regarding the piezoelectric materials as a promising biomaterial for guided bone regeneration application.

## DATA AVAILABILITY STATEMENT

The original contributions presented in the study are included in the article/Supplementary Material, further inquiries can be directed to the corresponding authors.

## AUTHOR CONTRIBUTIONS

SX, CL, and PL designed the study. YX and JC prepared the experimental materials. PZ and ZZ performed the experiments. MC and YH analyzed the experimental data. PZ wrote the original draft. SX, CL, and PL reviewed and edited the original manuscript. All authors participated in the revision of the draft and approved the final version of the manuscript.

## FUNDING

This study was financially supported by the Medical Research Foundation of Guangdong Province, China (A2018485), the Technology Research and Cultivation project of the Stomatological Hospital of Southern Medical University, China (PY2020011) and (PY2021003), and the Scientific Research Program of Traditional Chinese Medicine of Guangdong Province, China (20211274).

## REFERENCES

Amengual-Peñafiel, L., Brañes-Aroca, M., Marchesani-Carrasco, F., Jara-Sepúlveda, M. C., Parada-Pozas, L., and Cartes-Velásquez, R. (2019). Coupling between Osseointegration and Mechanotransduction to Maintain Foreign Body Equilibrium in the Long-Term: A Comprehensive Overview. *Jcm* 8 (2), 139. doi:10.3390/jcm8020139

Bai, Y., Dai, X., Yin, Y., Wang, J., Sun, X., Liang, W., et al. (2019). Biomimetic Piezoelectric Nanocomposite Membranes Synergistically Enhance Osteogenesis of Deproteinized Bovine Bone Grafts. *Ijn* 14, 3015–3026. doi:10.2147/ijn.S197824

Balbinot, G. D. S., Bahlis, E. A. D. C., Visioli, F., Leitune, V. C. B., Soares, R. M. D., and Collares, F. M. (2021). Polybutylene-adipate-terephthalate and Niobium-Containing Bioactive Glasses Composites: Development of Barrier Membranes with Adjusted Properties for Guided Bone Regeneration. *Mater. Sci. Eng. C* 125, 112115. doi:10.1016/j.msec.2021.112115

Biguetti, C. C., Cavalla, F., Fonseca, A. C., Tabanez, A. P., Siddiqui, D. A., Wheelis, S. E., et al. (2021). Effects of Titanium Corrosion Products on *In Vivo* Biological Response: A Basis for the Understanding of Osseointegration Failures Mechanisms. *Front. Mater.* 8, 651970. doi:10.3389/fmats.2021.651970

Brodbeck, W. G., Nakayama, Y., Matsuda, T., Colton, E., Ziats, N. P., and Anderson, J. M. (2002). Biomaterial Surface Chemistry Dictates Adherent Monocyte/macrophage Cytokine Expression *In Vitro*. *Cytokine* 18 (6), 311–319. doi:10.1006/cyto.2002.1048

Brown, B. N., Haschak, M. J., Lopresti, S. T., and Stahl, E. C. (2017). Effects of Age-Related Shifts in Cellular Function and Local Microenvironment upon the Innate Immune Response to Implants. *Semin. Immunol.* 29, 24–32. doi:10.1016/j.smim.2017.05.001

Cangellaris, O. V., and Gillette, M. U. (2018). Biomaterials for Enhancing Neuronal Repair. *Front. Mater.* 5, 225. doi:10.3389/fmats.2018.00021

Casey, L. M., Kakade, S., Decker, J. T., Rose, J. A., Deans, K., Shea, L. D., et al. (2019). Cargo-less Nanoparticles Program Innate Immune Cell Responses to Toll-like Receptor Activation. *Biomaterials* 218, 119333. doi:10.1016/j.biomaterials.2019.119333

Chakraborty, P., Dipankar, P., Dash, S. P., PriyaSrivastava, S., Srivastava, S., Dhyani, R., et al. (2020). Electrostatic Surface Potential of Macrophages Correlates with Their Functional Phenotype. *Inflammation* 43 (2), 641–650. doi:10.1007/s10753-019-01146-3

Chen, W., Yu, Z., Pang, J., Yu, P., Tan, G., and Ning, C. (2017). Fabrication of Biocompatible Potassium Sodium Niobate Piezoelectric Ceramic as an Electroactive Implant. *Materials* 10 (4), 345. doi:10.3390/ma10040345

Chen, Z., Visalakshan, R. M., Guo, J., Wei, F., Zhang, L., Chen, L., et al. (2019). Plasma Deposited Poly-Oxazoline Nanotextured Surfaces Dictate Osteoimmunomodulation towards Ameliorative Osteogenesis. *Acta Biomater.* 96, 568–581. doi:10.1016/j.actbio.2019.06.058

Chen, X., Wang, M., Chen, F., Wang, J., Li, X., Liang, J., et al. (2020). Correlations between Macrophage Polarization and Osteoinduction of Porous Calcium Phosphate Ceramics. *Acta Biomater.* 103, 318–332. doi:10.1016/j.actbio.2019.12.019

Chudinova, E. A., Surmeneva, M. A., Timin, A. S., Karpov, T. E., Wittmar, A., Ulbricht, M., et al. (2019). Adhesion, Proliferation, and Osteogenic Differentiation of Human Mesenchymal Stem Cells on Additively Manufactured Ti6Al4V alloy Scaffolds Modified with Calcium Phosphate Nanoparticles. *Colloids Surf. B: Biointerfaces* 176, 130–139. doi:10.1016/j.colsurfb.2018.12.047

Cipriano, A. F., Sallee, A., Guan, R.-G., Zhao, Z.-Y., Tayoba, M., Sanchez, J., et al. (2015). Investigation of Magnesium-Zinc-Calcium Alloys and Bone Marrow Derived Mesenchymal Stem Cell Response in Direct Culture. *Acta Biomater.* 12, 298–321. doi:10.1016/j.actbio.2014.10.018

Dai, X., Heng, B. C., Bai, Y., You, F., Sun, X., Li, Y., et al. (2021). Restoration of Electrical Microenvironment Enhances Bone Regeneration under Diabetic Conditions by Modulating Macrophage Polarization. *Bioactive Mater.* 6 (7), 2029–2038. doi:10.1016/j.bioactmat.2020.12.020

Ding, J., Venkatesan, R., Zhai, Z., Muhammad, W., Nakkala, J. R., and Gao, C. (2020). Micro- and Nanoparticles-Based Immunoregulation of Macrophages for Tissue Repair and Regeneration. *Colloids Surf. B: Biointerfaces* 192, 111075. doi:10.1016/j.colsurfb.2020.111075

Dubey, A. K., and Basu, B. (2014). Pulsed Electrical Stimulation and Surface Charge Induced Cell Growth on Multistage Spark Plasma Sintered Hydroxyapatite-Barium Titanate Piezobiocomposite. *J. Am. Ceram. Soc.* 97 (2), 481–489. doi:10.1111/jace.12647

Fahlgren, A., Bratengeier, C., Gelmi, A., Semeins, C. M., Klein-Nulend, J., Jager, E. W. H., et al. (2015). Biocompatibility of Polypyrrole with Human Primary Osteoblasts and the Effect of Dopants. *Plos One* 10 (7), e0134023. doi:10.1371/journal.pone.0134023

Fonseca, J. H., Bagne, L., Meneghetti, D. H., Santos, G. M. T., Esquisatto, M. A. M., Andrade, T. A. M., et al. (2019). Electrical Stimulation: Complementary Therapy to Improve the Performance of Grafts in Bone Defects. *J. Biomed. Mater. Res.* 107 (4), 924–932. doi:10.1002/jbm.b.34187

Gorodzha, S. N., Muslimov, A. R., Syromotina, D. S., Timin, A. S., Tcvetkov, N. Y., Lepik, K. V., et al. (2017). A Comparison Study between Electrospun Polycaprolactone and Piezoelectric Poly(3-Hydroxybutyrate-Co-3-Hydroxyvalerate) Scaffolds for Bone Tissue Engineering. *Colloids Surf. B: Biointerfaces* 160, 48–59. doi:10.1016/j.colsurfb.2017.09.004

Hamlet, S. M., Lee, R. S. B., Moon, H. J., Alfarsi, M. A., and Ivanovski, S. (2019). Hydrophilic Titanium Surface-induced Macrophage Modulation Promotes Pro-osteogenic Signalling. *Clin. Oral Impl Res.* 30 (11), 1085–1096. doi:10.1111/clr.13522

Hassler, C. R., Rybicki, E. F., Diegle, R. B., and Clark, L. C. (1977). Studies of Enhanced Bone Healing via Electrical Stimuli. *Clin. Orthopaedics Relat. Res.* (124), 9–19. doi:10.1097/00003086-197705000-00003

He, X.-T., Li, X., Yin, Y., Wu, R.-X., Xu, X.-Y., and Chen, F.-M. (2018). The Effects of Conditioned media Generated by Polarized Macrophages on the Cellular Behaviours of Bone Marrow Mesenchymal Stem Cells. *J. Cel. Mol. Med.* 22 (2), 1302–1315. doi:10.1111/jcmm.13431

Hotchkiss, K. M., Reddy, G. B., Hyzy, S. L., Schwartz, Z., Boyan, B. D., and Olivares-Navarrete, R. (2016). Titanium Surface Characteristics, Including Topography and Wettability, Alter Macrophage Activation. *Acta Biomater.* 31, 425–434. doi:10.1016/j.actbio.2015.12.003

Hynes, R. (1987). Integrins: a Family of Cell Surface Receptors. *Cell* 48 (4), 549–554. doi:10.1016/0092-8674(87)90233-9

Isaacson, B. M., and Bloebaum, R. D. (2010). Bone Bioelectricity: what Have We Learned in the Past 160 Years. *J. Biomed. Mater. Res.* 95A (4), 1270–1279. doi:10.1002/jbm.a.32905

Jin, S.-S., He, D.-Q., Luo, D., Wang, Y., Yu, M., Guan, B., et al. (2019). A Biomimetic Hierarchical Nanointerface Orchestrates Macrophage Polarization and Mesenchymal Stem Cell Recruitment to Promote Endogenous Bone Regeneration. *Acs Nano* 13 (6), 6581–6595. doi:10.1021/acsnano.9b00489

Kang, H., Kim, S., Wong, D. S. H., Jung, H. J., Lin, S., Zou, K., et al. (2017). Remote Manipulation of Ligand Nano-Oscillations Regulates Adhesion and Polarization of Macrophages *In Vivo*. *Nano Lett.* 17 (10), 6415–6427. doi:10.1021/acs.nanolett.7b03405

Khare, D., Basu, B., and Dubey, A. K. (2020). Electrical Stimulation and Piezoelectric Biomaterials for Bone Tissue Engineering Applications. *Biomaterials* 258, 120280. doi:10.1016/j.biomaterials.2020.120280

Kim, J., Kim, H.-s., and Park, C. H. (2016). Contribution of Surface Energy and Roughness to the Wettability of Polyamide 6 and Polypropylene Film in the Plasma-Induced Process. *Textile Res. J.* 86 (5), 461–471. doi:10.1177/0040517515580511

Kong, Y., Liu, F., Ma, B., Duan, J., Yuan, W., Sang, Y., et al. (2021). Wireless Localized Electrical Stimulation Generated by an Ultrasound-Driven Piezoelectric Discharge Regulates Proinflammatory Macrophage Polarization. *Adv. Sci.* 8 (13), 2100962. doi:10.1002/advs.202100962

Kumar S, S., and Hiremath, S. S. (2019). Effect of Surface Roughness and Surface Topography on Wettability of Machined Biomaterials Using Flexible Viscoelastic Polymer Abrasive media. *Surf. Topogr.: Metrol. Prop.* 7 (1), 015004. doi:10.1088/2051-672X/aaf6f6

Lee, J.-H., Hinchet, R., Kim, T. Y., Ryu, H., Seung, W., Yoon, H.-J., et al. (2015). Control of Skin Potential by Triboelectrification with Ferroelectric Polymers. *Adv. Mater.* 27 (37), 5553–5558. doi:10.1002/adma.201502463

Liu, Y., Chen, X., Wang, L., Yang, T., Yuan, Q., and Ma, G. (2014). Surface Charge of PLA Microparticles in Regulation of Antigen Loading, Macrophage Phagocytosis and Activation, and Immune Effects *In Vitro*. *Particuology* 17, 74–80. doi:10.1016/j.partic.2014.02.006

Liu, Y., Zhang, X., Cao, C., Zhang, Y., Wei, J., Li, Y. j., et al. (2017). Built-In Electric Fields Dramatically Induce Enhancement of Osseointegration. *Adv. Funct. Mater.* 27 (47), 1703771. doi:10.1002/adfm.201703771

Marchesano, V., Gennari, O., Mecozzi, L., Grilli, S., and Ferraro, P. (2015). Effects of Lithium Niobate Polarization on Cell Adhesion and Morphology. *ACS Appl. Mater. Inter.* 7 (32), 18113–18119. doi:10.1021/acsami.5b05340

McWhorter, F. Y., Wang, T., Nguyen, P., Chung, T., and Liu, W. F. (2013). Modulation of Macrophage Phenotype by Cell Shape. *Proc. Natl. Acad. Sci.* 110 (43), 17253–17258. doi:10.1073/pnas.1308887110

Miron, R. J., and Bosshardt, D. D. (2016). OsteoMacs: Key Players Around Bone Biomaterials. *Biomaterials* 82, 1–19. doi:10.1016/j.biomaterials.2015.12.017

Neacsu, P., Mazare, A., Cimpean, A., Park, J., Costache, M., Schmuki, P., et al. (2014). Reduced Inflammatory Activity of RAW 264.7 Macrophages on Titania Nanotube Modified Ti Surface. *Int. J. Biochem. Cel Biol.* 55, 187–195. doi:10.1016/j.biocel.2014.09.006

Ogle, M. E., Segar, C. E., Sridhar, S., and Botchwey, E. A. (2016). Monocytes and Macrophages in Tissue Repair: Implications for Immunoregenerative Biomaterial Design. *Exp. Biol. Med. (Maywood)* 241 (10), 1084–1097. doi:10.1177/1535370216650293

Omar, O., Elgali, I., Dahlin, C., and Thomsen, P. (2019). Barrier Membranes: More Than the Barrier Effect. *J. Clin. Periodontol.* 46, 103–123. doi:10.1111/jcpe.13068

Peng, H., Li, J., Xu, Y., and Lv, G. (2020). Icaritin Enhancing Bone Formation Initiated by Sub-microstructured Calcium Phosphate Ceramic for Critical Size Defect Repair. *Front. Mater.* 7, 598057. doi:10.3389/fmats.2020.598057

Purohit, S. D., Singh, H., Bhaskar, R., Yadav, I., Bhushan, S., Gupta, M. K., et al. (2020). Fabrication of Graphene Oxide and Nanohydroxyapatite Reinforced

Gelatin-Alginate Nanocomposite Scaffold for Bone Tissue Regeneration. *Front. Mater.* 7, 250. doi:10.3389/fmats.2020.00250

Rajabi, A. H., Jaffe, M., and Arinzeh, T. L. (2015). Piezoelectric Materials for Tissue Regeneration: A Review. *Acta Biomater.* 24, 12–23. doi:10.1016/j.actbio.2015.07.010

Ribeiro, S., Puckert, C., Ribeiro, C., Gomes, A. C., Higgins, M. J., and Lanceros-Méndez, S. (2020). Surface Charge-Mediated Cell-Surface Interaction on Piezoelectric Materials. *ACS Appl. Mater. Inter.* 12 (1), 191–199. doi:10.1021/acsami.9b17222

Rohde, M., Ziebart, J., Kirschstein, T., Sellmann, T., Porath, K., Kühl, F., et al. (2019). Human Osteoblast Migration in DC Electrical Fields Depends on Store Operated Ca2+-Release and Is Correlated to Upregulation of Stretch-Activated TRPM7 Channels. *Front. Bioeng. Biotechnol.* 7, 422. doi:10.3389/fbioe.2019.00422

Sadowska, J. M., and Ginebra, M.-P. (2020). Inflammation and Biomaterials: Role of the Immune Response in Bone Regeneration by Inorganic Scaffolds. *J. Mater. Chem. B* 8 (41), 9404–9427. doi:10.1039/d0tb01379j

Salamanca, E., Tsao, T.-C., Hseuh, H.-W., Wu, Y.-F., Choy, C.-S., Lin, C.-K., et al. (2021). Fabrication of Polylactic Acid/β-Tricalcium Phosphate FDM 3D Printing Fiber to Enhance Osteoblastic-like Cell Performance. *Front. Mater.* 8, 683706. doi:10.3389/fmats.2021.683706

Sasaki, J.-I., Abe, G. L., Li, A., Thongthai, P., Tsuboi, R., Kohno, T., et al. (2021). Barrier Membranes for Tissue Regeneration in Dentistry. *Biomaterial Invest. Dentistry* 8 (1), 54–63. doi:10.1080/26415275.2021.1925556

Seebach, E., and Kubatzky, K. F. (2019). Chronic Implant-Related Bone Infections-Can Immune Modulation Be a Therapeutic Strategy. *Front. Immunol.* 10, 1724. doi:10.3389/fimmu.2019.01724

Tandon, B., Blaker, J. J., and Cartmell, S. H. (2018). Piezoelectric Materials as Stimulatory Biomedical Materials and Scaffolds for Bone Repair. *Acta Biomater.* 73, 1–20. doi:10.1016/j.actbio.2018.04.026

Tang, Y., Wu, C., Wu, Z., Hu, L., Zhang, W., and Zhao, K. (2017). Fabrication and *In Vitro* Biological Properties of Piezoelectric Bioceramics for Bone Regeneration. *Sci. Rep.* 7, 43360. doi:10.1038/srep43360

Tang, Z.-h., Su, S., Liu, Y., Zhu, W.-q., Zhang, S.-m., and Qiu, J. (2021). Hydrothermal Synthesis of Zinc-Incorporated Nano-Cluster Structure on Titanium Surface to Promote Osteogenic Differentiation of Osteoblasts and hMSCs. *Front. Mater.* 8, 739071. doi:10.3389/fmats.2021.739071

Teixeira, L. N., Crippa, G. E., Gimenes, R., Zaghete, M. A., de Oliveira, P. T., Rosa, A. L., et al. (2011). Response of Human Alveolar Bone-Derived Cells to a Novel Poly(vinylidene Fluoride-Trifluoroethylene)/barium Titanate Membrane. *J. Mater. Sci. Mater. Med.* 22 (1), 151–158. doi:10.1007/s10856-010-4189-z

Thangam, R., Kim, M. S., Bae, G., Kim, Y., Kang, N., Lee, S., et al. (2021). Remote Switching of Elastic Movement of Decorated Ligand Nanostructures Controls the Adhesion-Regulated Polarization of Host Macrophages. *Adv. Funct. Mater.* 31 (21), 2008698. doi:10.1002/adfm.202008698

Toledano-Osorio, M., Manzano-Moreno, F. J., Ruiz, C., Toledano, M., and Osorio, R. (2021). Testing Active Membranes for Bone Regeneration: A Review. *J. Dentistry* 105, 103580. doi:10.1016/j.jdent.2021.103580

Vallés, G., Bensiamar, F., Maestro-Paramio, L., García-Rey, E., Vilaboa, N., and Saldaña, L. (2020). Influence of Inflammatory Conditions provided by Macrophages on Osteogenic Ability of Mesenchymal Stem Cells. *Stem Cel Res. Ther.* 11 (1), 57. doi:10.1186/s13287-020-1578-1

Vaněk, P., Kolská, Z., Luxbacher, T., García, J. A. L., Lehocký, M., Vandrovcová, M., et al. (2016). Electrical Activity of Ferroelectric Biomaterials and its Effects on the Adhesion, Growth and Enzymatic Activity of Human Osteoblast-like Cells. *J. Phys. D: Appl. Phys.* 49 (17), 175403. doi:10.1088/0022-3727/49/17/175403

Wang, J., Li, S.-F., Wang, T., Sun, C.-H., Wang, L., Huang, M.-J., et al. (2017). Isopsoralen-mediated Suppression of Bone Marrow Adiposity and Attenuation of the Adipogenic Commitment of Bone Marrow-Derived Mesenchymal Stem Cells. *Int. J. Mol. Med.* 39 (3), 527–538. doi:10.3892/ijmm.2017.2880

Wang, W., Li, J., Liu, H., and Ge, S. (2020). Advancing Versatile Ferroelectric Materials toward Biomedical Applications. *Adv. Sci.* 8 (1), 2003074. doi:10.1002/advs.202003074

Wang, X., Mei, L., Jiang, X., Jin, M., Xu, Y., Li, J., et al. (2021a). Hydroxyapatite-Coated Titanium by Micro-arc Oxidation and Steam-Hydrothermal Treatment Promotes Osseointegration. *Front. Bioeng. Biotechnol.* 9, 625877. doi:10.3389/fbioe.2021.625877

Wang, Z., He, X., Tang, B., Chen, X., Dong, L., Cheng, K., et al. (2021b). Polarization Behavior of Bone Marrow-Derived Macrophages on Charged P(VDF-TrFE) Coatings. *Biomater. Sci.* 9 (3), 874–881. doi:10.1039/d0bm01604g

Wei, F., Zhou, Y., Wang, J., Liu, C., and Xiao, Y. (2018). The Immunomodulatory Role of BMP-2 on Macrophages to Accelerate Osteogenesis. *Tissue Eng. A* 24 (7-8), 584–594. doi:10.1089/ten.tea.2017.0232

Wu, J., Yu, P., Lv, H., Yang, S., and Wu, Z. (2020). Nanostructured Zirconia Surfaces Regulate Human Gingival Fibroblasts Behavior through Differential Modulation of Macrophage Polarization. *Front. Bioeng. Biotechnol.* 8, 611684. doi:10.3389/fbioe.2020.611684

Xie, Y., Hu, C., Feng, Y., Li, D., Ai, T., Huang, Y., et al. (2020). Osteoimmunomodulatory Effects of Biomaterial Modification Strategies on Macrophage Polarization and Bone Regeneration. *Regener. Biomater.* 7 (3), 233–245. doi:10.1093/rb/rbaa006

Xu, D., Qian, J., Guan, X., Ren, L., Yang, K., Huang, X., et al. (2020). Copper-Containing Alloy as Immunoregulatory Material in Bone Regeneration via Mitochondrial Oxidative Stress. *Front. Bioeng. Biotechnol.* 8, 620629. doi:10.3389/fbioe.2020.620629

Yang, L., Xiao, L., Gao, W., Huang, X., Wei, F., Zhang, Q., et al. (2021a). Macrophages at Low-Inflammatory Status Improved Osteogenesis *via* Autophagy Regulation. *Tissue Eng. Part A* Epub ahead of print. doi:10.1089/ten.tea.2021.0015

Yang, Y., Lin, Y., Zhang, Z., Xu, R., Yu, X., and Deng, F. (2021b). Micro/nano-net Guides M2-Pattern Macrophage Cytoskeleton Distribution via Src-ROCK Signalling for Enhanced Angiogenesis. *Biomater. Sci.* 9 (9), 3334–3347. doi:10.1039/d1bm00116g

Yang, Y., Zhang, T., Jiang, M., Yin, X., Luo, X., and Sun, H. (2021c). Effect of the Immune Responses Induced by Implants in a Integrated Three-dimensional Micro-nano Topography on Osseointegration. *J. Biomed. Mater. Res.* 109 (8), 1429–1440. doi:10.1002/jbm.a.37134

Zhang, C., Liu, W., Cao, C., Zhang, F., Tang, Q., Ma, S., et al. (2018). Modulating Surface Potential by Controlling the β Phase Content in Poly(vinylidene Fluoridetrifluoroethylene) Membranes Enhances Bone Regeneration. *Adv. Healthc. Mater.* 7 (11), 1701466. doi:10.1002/adhm.201701466

Zhang, W., Lu, X., Yuan, Z., Shen, M., Song, Y., Liu, H., et al. (2019). Establishing an Osteoimmunomodulatory Coating Loaded with Aspirin on the Surface of Titanium Primed with Phase-Transited Lysozyme. *Ijn* 14, 977–991. doi:10.2147/ijn.S190766

Zhang, W., Cao, S., Liang, S., Tan, C. H., Luo, B., Xu, X., et al. (2020). Differently Charged Super-paramagnetic Iron Oxide Nanoparticles Preferentially Induced M1-like Phenotype of Macrophages. *Front. Bioeng. Biotechnol.* 8, 537. doi:10.3389/fbioe.2020.00537

Zhou, Z., Li, W., He, T., Qian, L., Tan, G., and Ning, C. (2016). Polarization of an Electroactive Functional Film on Titanium for Inducing Osteogenic Differentiation. *Sci. Rep.* 6, 35512. doi:10.1038/srep35512

**Conflict of Interest:** The authors declare that the research was conducted in the absence of any commercial or financial relationships that could be construed as a potential conflict of interest.

**Publisher's Note:** All claims expressed in this article are solely those of the authors and do not necessarily represent those of their affiliated organizations, or those of the publisher, the editors and the reviewers. Any product that may be evaluated in this article, or claim that may be made by its manufacturer, is not guaranteed or endorsed by the publisher.